[8] C.-H. Tseng and T.-H. Chu, "Measurement of frequency-dependent equivalent width of substrate integrated waveguide," *IEEE Trans. Microw. Theory Techn.*, vol. 54, no. 4, pp. 1431–1437, Jun. 2006.
[9] P. Chen, W. Hong, Z. Kuai, and J. Xu, "A substrate integrated waveguide circular polarized slot radiator and its linear array," *IEEE Antennas Wireless Propag. Lett.*, vol. 8, pp. 120–123, 2009.
[10] Y. Dong and T. Itoh, "Miniaturized substrate integrated waveguide slot antennas based on negative order resonance," *IEEE Trans. Antennas Propag.*, vol. 58, no. 12, pp. 3856–3864, Dec. 2010.
[11] L. S. Wu, X. L. Zhou, Q. F. Wei, and W. Y. Yin, "An extended doublet substrate integrated waveguide (SIW) bandpass filter with a complementary split ring resonator (CSRR)," *IEEE Microw. Wireless Compon. Lett.*, vol. 19, no. 12, pp. 777–779, Dec. 2009.
[12] S. Sam and S. Lim, "Electrically small eighth-mode substrate-integrated waveguide (EMSIW) antenna with different resonant frequencies depending on rotation of complementary split ring resonator," *IEEE Trans. Antennas Propag.*, vol. 61, no. 10, pp. 4933–4939, Oct. 2013.
[13] D. K. Cheng, *Field and Wave Electromagnetics*. New York, NY, USA: Addison-Wesley, 1989.
[14] Y. J. Cheng, W. Hong, and K. Wu, "Millimeter-wave half mode substrate integrated waveguide frequency scanning antenna with quadri-polarization," *IEEE Trans. Antennas Propag.*, vol. 58, no. 6, pp. 1848–1855, Jun. 2010.
[15] R. F. Xu, B. S. Izquierdo, and P. R. Young, "Switchable substrate integrated waveguide," *IEEE Microw. Wireless Compon. Lett.*, vol. 21, no. 4, pp. 194–196, Apr. 2011.
[16] Y. Dong and T. Itoh, "Composite right/left-handed substrate integrated waveguide and half mode substrate integrated waveguide leaky-wave structures," *IEEE Trans. Antennas Propag.*, vol. 59, no. 3, pp. 767–775, Mar. 2011.
[17] B. Liu, W. Hong, Y.-Q. Wang, Q.-H. Lai, and K. Wu, "Half mode substrate integrated waveguide (HMSIW) 3-dB coupler," *IEEE Microw. Wireless Compon. Lett.*, vol. 17, no. 1, pp. 22–24, Jan. 2007.
[18] S. Zhang, T.-J. Bian, Y. Zhai, W. Liu, G. Yang, and F.-L. Liu, "Quarter substrate integrated waveguide resonator applied to fractal-shaped BPFs," *Microw. J.*, vol. 55, no. 5, pp. 200–208, May 2012.
[19] J.-M. Kim, M. Han, and H. Sohn, "Magnetic resonance-based wireless power transmission through concrete structures," *J. Electromagn. Eng. Sci.*, vol. 15, no. 2, pp. 104–110, Apr. 2015.
[20] Y. J. Chen, X. Y. Xue, Y. G. Wang, and T. H. Wang, "Synthesis and ethanol sensing characteristics of single crystalline SnO_2 nanorods," *Appl. Phys. Lett.*, vol. 87, no. 23, p. 233503, 2005.
[21] T.-J. Hsueh, C.-L. Hsu, S.-J. Chang, and I.-C. Chen, "Laterally grown ZnO nanowire ethanol gas sensors," *Sens. Actuators B, Chem.*, vol. 126, no. 2, pp. 473–477, Oct. 2007.
[22] Y. Kwon *et al.*, "Enhanced ethanol sensing properties of TiO_2 nanotube sensors," *Sens. Actuators B, Chem.*, vol. 173, pp. 441–446, Oct. 2012.
[23] S. Brahim, S. Colbern, R. Gump, A. Moser, and L. Grigorian, "Carbon nanotube-based ethanol sensors," *Nanotechnology*, vol. 20, no. 23, p. 235502, May 2009.
[24] *Ethanol Product Information*. [Online]. Available: http://www.sigmaaldrich.com/

Millimeter-Wave Thin Lens Employing Mixed-Order Elliptic Filter Arrays

Jungsuek Oh

***Abstract*— This communication presents a novel approach for designing a simplified and cost-effective millimeter-wave thin lens by reducing the number of substrates and metal layers for a given tunable range of the phase shift. It is demonstrated that this can be achieved by employing mixed-order elliptic filter arrays where the different orders of the filter are responsible for different tunable ranges of the phase shift. The key features of the elliptic filters and their mixed-order array are introduced. It is found that constructively utilizing the interlayer coupling between the metal layers renders an elliptic filter response, and the mixed-order configuration of the elliptic filter array can be utilized to design the devised thin lens. The design procedure for the affordable thin lens configuration is discussed. The empirical and simulated results demonstrate that the conventional planar lens can be further simplified in terms of the number of substrates and metal layers, maintaining the tunable range of the phase shift. It is confirmed that the fabricated mixed-order lens is less than 0.05 $\lambda 0$ in total thickness and has a gain of up to 12 dB with $f/D = 0.7$.**

***Index Terms*— Elliptic filters, lenses, millimeter-wave antennas.**

I. Introduction

Lenses are instrumental for accurate beam shaping as they are capable of transforming the incident propagating electromagnetic (EM) wavefronts into a desired form. In recent years, lenses have been particularly favored in the wireless community for the purpose of gain enhancement for large-scale antenna applications [1], [2]. Lenses can improve the system gain efficiently when feed losses increase with an increase in the number of antenna elements. The advantages of employing lenses are especially evident in large-scale phased arrays in which the array gain deteriorates beyond a finite number of antenna elements owing to excessive insertion losses caused by the interconnections. However, there is a definite tradeoff in terms of system complexity from the point of view of the device bill of materials because of the addition of a sophisticated lens. A typical lens comprises dielectric media where the curved surface topology renders an optimized phase shift for each of the respective coordinates on the lens to collectively construct the desired wave form [3], [4]. Despite the excellent beam shaping characteristics of the aforementioned concave and convex microwave lenses, their usage in millimeter-wave mass-market applications like small-cell access points and backhauls have been relatively stagnant mostly owing to their bulky profile and stringent tolerance to errors during fabrication.

As an alternate solution, it has been reported that the focusing operation of the lens can be obtained by an appropriate arrangement of the planar metallic resonant unit cells that can devise various phase shifts. In a previous study of this lens structure, the metallic unit cell was composed of two antennas and a filter where the first antenna captured the propagating EM waves and the filter added a specific phase shift. The second antenna reradiated the modified EM waves

Manuscript received May 24, 2015; revised April 6, 2016; accepted April 17, 2016. Date of publication April 27, 2016; date of current version July 5, 2016. This work was supported in part by Samsung Research America, in part by Inha University under Grant INHA-53353, and in part by the Basic Science Research Program through the National Research Foundation of Korea within the Ministry of Science, ICT & Future Planning under Grant NRF-2015R1C1A1A01055487.

The author is with the Department of Electronic Engineering, Inha University, Incheon 402-751, South Korea (e-mail: jungsuek@inha.ac.kr).

Color versions of one or more of the figures in this communication are available online at http://ieeexplore.ieee.org.

Digital Object Identifier 10.1109/TAP.2016.2559582

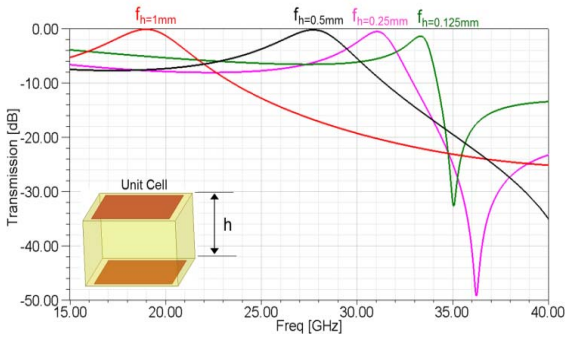

Fig. 1. Frequency response of the low-pass unit cell as a function of h.

into free space [5], [6]. The planar configuration of this lens structure provided a substantial geometrical advantage, as its design and system integration are straightforward. However, the profile of the unit cell that consists of two antennas and a filter was excessively bulky to achieve an efficient beam focusing methodology.

Recent advancements in frequency-selective surface (FSS) techniques can synthesize accurate spatial filter responses owing to a relatively large degree of design freedom in controlling the profile of the EM waves [7]. The utilization of EM in-plane couplings with nearby unit cells results in electrically small and thin spatial filter unit cells. This in-plane coupling also aids the simplification of the unit cell structure. The combination of FSS-based spatial filters having different dimensions responsible for different levels of phase shift has been proposed for a lens-based beam shaping in [8]–[10]. This type of FSS-based lens contains several substrates and metal layers to realize the required filter response. The electrically miniaturized configuration of the FSS lens can result in more compact and higher gain antenna systems. However, the alternate arrangement of the substrates and metal layers adhesively connected via bonding layers requires considerable levels of fabrication precision that is ultimately correlated to the antenna performance at high carrier frequencies.

This communication presents novel design techniques that can simplify the required lamination profiles without affecting the antenna beam focusing accuracy and efficiency through realization of elliptic spatial filter responses and their mixed-order combinations. It is demonstrated that the proposed design can provide moderate beam shaping and bandwidth features. In Section II, unit cells having elliptic spatial filter responses and their novel mixed-order combinations enabling low-cost thin lens designs are presented. The expected features of the whole lens structure are discussed by performing full-wave EM simulations. In Section III, the performance of the proposed lens is demonstrated through measurements of the fabricated samples with a reliable setup. Finally, the performance of the proposed lens is compared with that of a lens specified in a previous study, designed by uniform-order FSS spatial filters with more complex features.

II. Thin Lens Using Mixed-Order Elliptic Filter Arrays

A. Elliptic Spatial Filter Array

This section presents the features of the unit cell that renders an elliptic spatial filter response. The frequency response of the low-pass unit cell element is viewed as a function of the thickness (h). Fig. 1 shows the frequency responses of the low-pass element consisting of two metallic patch layers connected through a substrate layer when h is 0.125, 0.25, 0.5, and 1 mm, respectively. The selected unit cell size is 1.6 mm × 1.6 mm, and the dielectric constant of the substrate is 10.2. The elliptic filter response of

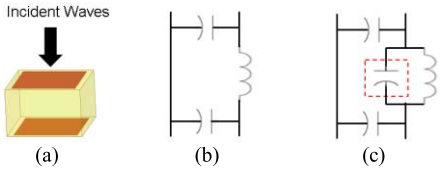

Fig. 2. (a) Conventional low-pass FSS unit cell, (b) its equivalent circuit, and (c) modified equivalent circuit exhibiting an elliptic filter response.

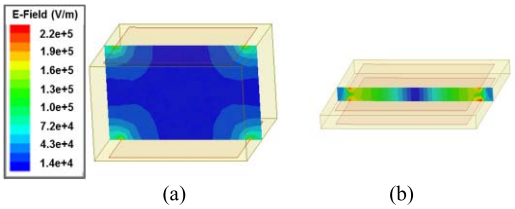

Fig. 3. E-fields of unit cells when (a) $h = 1$ mm and (b) $h = 0.125$ mm.

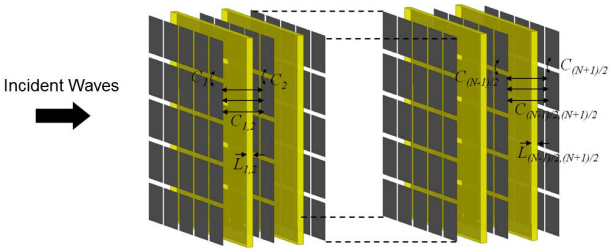

Fig. 4. Exploded view of the elliptic spatial filter array.

the designed unit cell is characterized using parametric studies. As the height h is decreased by a factor of two, the ratio of the previous operating frequency (f_h) with respect to the succeeding f_h varies at smaller degrees (<2). The ratios are calculated as $f_{h=0.5\,\mathrm{mm}}/f_{h=1\,\mathrm{mm}} = 1.46$, $f_{h=0.25\,\mathrm{mm}}/f_{h=0.5\,\mathrm{mm}} = 1.12$, and $f_{h=0.125\,\mathrm{mm}}/f_{h=0.25\,\mathrm{mm}} = 1.07$ that are smaller than the increase in the volume of the unit cell (=2). This is because of the fact that the increased interlayer coupling between the top and bottom patches offsets the increase in the f_h leading to miniaturization effects. This indicates that the variation in the attenuation zero of the unit cell is not linear when the volume of the unit cell is linearly decreased. Conventional low-pass FSS elements are found to be insufficient in interpreting this phenomenon.

Addition of a capacitance representing the interlayer couplings into the equivalent circuit of the conventional low-pass FSS elements produces an elliptic filter response. Fig. 2 shows conventional low-pass FSS unit cell, its equivalent circuit, and the modified equivalent circuit exhibiting an elliptic filter response. The capacitance in the red dashed box of Fig. 2(c) corresponds to the interlayer coupling. Fig. 3(a) and (b) depicts the increased interlayer coupling as a function of h. It should be noted that the aforementioned miniaturization effect is a result of a decrease in the bandwidth of the unit cell (increased quality factor), as shown in Fig. 1. This feature exhibits an advantage of the proposed mixed-order design approach that employs both the lower order wideband elements and the higher order narrowband elements rather than employing only the higher order narrowband elements. Fig. 4 describes all the possible EM couplings in the proposed elliptic spatial filter array. Their equivalent circuit is shown in Fig. 5, including the newly added capacitance $C_{(N-1)/2,(N+1)/2}$. When $N = 3$ (third-order elliptic filter), the transmission zero w_{pol} is given by (1). The interlayer

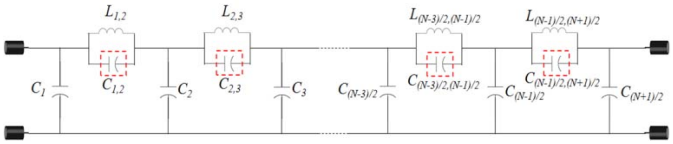

Fig. 5. Equivalent circuit of the elliptic spatial filter array in Fig. 4.

couplings ($C_{(N-1)/2,(N+1)/2}$) can be estimated by obtaining w_{pol} values from the full-wave EM simulation and using (2). It is assumed that the values of L and C in the conventional low-pass and bandpass filter prototypes are known, as derived in [12] and [13]. Based on the known features, this communication focuses on the introduction and derivation of the aforementioned interlayer capacitance and the novel array topology of the elliptic response. Based on the aforementioned discussions, a design procedure to synthesize an Nth-order elliptic FSS response is setup as shown in the following.

Step 1: A thin substrate ($\ll 0.1\ \lambda_0$) is selected to utilize the interlayer couplings. This communication selects a thickness of 0.023 λ_0. Typically, the freedom in the selection of high-frequency substrates with an extremely thin configuration is limited by the industrial standards of the PCB production.

Step 2: Initial patch sizes for the third-order low-pass response are determined by a known design procedure for the low-pass FSS unit cell to achieve the target frequency range [12], [13]. Through this step, initial values of C_1 and $L_{1,2}$ in Fig. 5 can be determined for the given substrate.

Step 3: Through a full-wave EM simulation of the initial unit cell, the transmission zero w_{pol} is determined and the interlayer capacitance $C_{1,2}$ can be extracted from (2).

Step 4: Assuming that slight changes in patch sizes do not cause significant changes in $C_{1,2}$, the characterized third-order elliptic unit cells are stacked and then the patch sizes are slightly adjusted to enable several w_{pol} to produce one passband, referring to known tables for lumped elements of the Nth-order elliptic low-pass filter [11]

$$W_{pol} = \sqrt{\frac{2Z_0^2C_1 - L_{1,2}}{Z_0^2L_{1,2}C_1(C_1+2C_{1,2})}} \quad \text{where } C_1 = C_2 \text{ (symmetry network)} \tag{1}$$

$$C_{1,2} = \frac{1}{w_{pol}L_{1,2}} - \frac{1}{2w_{pol}^2Z_0^2C_1} - \frac{C_1}{2}. \tag{2}$$

B. Mixed-Order Combinations of the Elliptic Spatial Filters

In conventional lens design employing a uniform-order spatial filter array, the tunable range of the phase shift is improved by increasing the order of the spatial filter. However, this increased order essentially requires many more substrates and bonding and metal layers leading to a significant rise in fabrication errors and costs. Fig. 6 presents the transmittance as a function of the patch size, where the third-order elliptic spatial filter unit cell consists of only two metal layers by merely eliminating the second metal layer from the fifth-order elliptic spatial filter unit cell. Fig. 7 shows the phase shifts in the passband of the elliptic spatial filters corresponding to the respective patch sizes. As it can be observed from Fig. 6, the cutoff slope of the third order is flatter than that of the fifth order, owing to an increase in the distance between the metal layers (decreased interlayer couplings) in a unit cell of fixed thickness with the removal of the second metal layer. In order to achieve wider bandwidth characteristics,

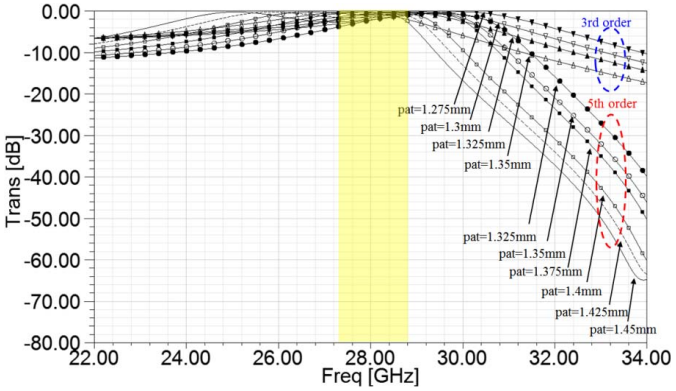

Fig. 6. Transmittance of the third- and fifth-order elliptic spatial filters as a function of the patch size (pat).

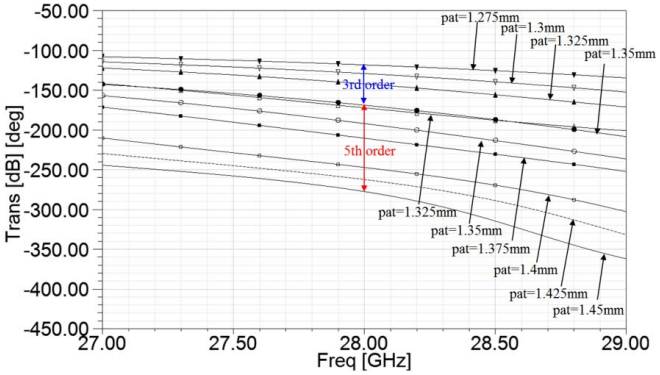

Fig. 7. Phase shifts of the third- and fifth-order elliptic spatial filters with different patch sizes (pat).

it is found that for an identical phase shift, it is effective to select lower order spatial filters owing to their flatter slope of transmittance. Therefore, rather than employing a uniform (single)-order spatial filter the utilization of more than two different-order (mixed-order) spatial filters enables the design of affordable thin lenses by reducing the required number of substrates, bonding and metal layers. This feature of the proposed design approach can be demonstrated by achieving the same tunable range of the phase shift as a conventional lens design employing many more substrates and bonding and metal layers. In this context, Fig. 7 demonstrates that the two different-order (third and fifth) elliptic spatial filters can cover different ranges of phase shifts; their combination covers an approximate tunable range of 170°. This is similar to the tunable range of the previously reported third-order bandpass FSS spatial filters that consist of three substrates and two bonding and four metal layers. In comparison, the proposed mixed-order elliptic spatial filters require only two substrates and one bonding and three metal layers.

Table I lists the patch sizes, phase shift, and insertion losses of the third- and fifth-order elliptic spatial filters discussed in Figs. 6 and 7. Finally, Fig. 8 shows the exploded conceptual view of the proposed lens employing mixed-order elliptic spatial filter arrays, where the second metal layer is partially removed to realize a lower order (third) elliptic spatial filter response.

C. Design of an Ultrathin Convex Lens

This section presents the design of an ultrathin convex lens employing mixed-order elliptic spatial filter arrays. Based on the discussions in Sections II-A and II-B, a design procedure for the proposed lens is set up as shown in the following.

TABLE I

PATCH SIZE, PHASE SHIFT, AND INSERTION LOSS OF THE THIRD- AND FIFTH-ORDER ELLIPTIC SPATIAL FILTERS

UC#	Order	P1 (mm)	P2 (mm)	P3 (mm)	Phase (deg)	IL (dB)
1	5th	1.45	1.5	1.45	-278	1.8
2	5th	1.425	1.5	1.425	-262	1.6
3	5th	1.4	1.5	1.4	-247	1
4	5th	1.375	1.5	1.375	-211	0.4
5	5th	1.35	1.5	1.35	-192	0.8
6	3rd	1.35	N/A	1.35	-169	0.8
7	3rd	1.325	N/A	1.325	-145	0.5
8	3rd	1.3	N/A	1.3	-130	1.2
9	3rd	1.275	N/A	1.275	-114	1.5

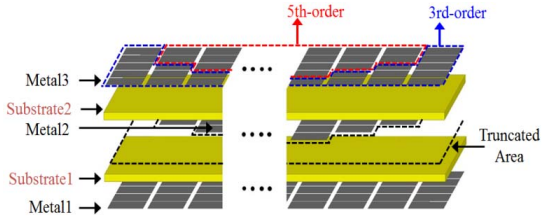

Fig. 8. Exploded conceptual view of the proposed lens employing mixed-order elliptic spatial filter arrays.

Step 1: The target distance between the lens, the antenna source, and the aperture are first selected as per the system requirements. In this communication, the target distance and aperture area are selected to be 35 mm and 51.2 mm $\times$ 51.2 mm, respectively. A $\lambda/2$ dipole antenna is selected as the antenna source. Please note that the target distance determines the needed tunable range of the phase shift. For example, 35 mm in this communication determines the tunable range of the phase shift to be 163° [$=-101-(-274)$] for the selected aperture, as shown in Table II.

Step 2: Phase profiles of the propagating wavefront emitted from the source are captured over the selected aperture at the selected distance. In this communication, considering the unit cell size (1.6 mm), the phase profiles are captured at every 3.2 mm from the center of the lens.

Step 3: The required phase shifts are calculated at all the points to realize a uniformly flat wavefront of plane waves. Based on the predetermined phase shifts, the dimension profiles of the unit cells at each point are selected from Table I. When the unit cell at a point is the same type as the unit cell at the next point, the areas occupied by the two unit cells are grouped and are called a zone.

Step 4: To achieve the required tunable range of the phase shift, the requisite orders of the elliptic FSS responses are determined for the given elliptic FSS unit cells and their mixed-order combinations (Sections II-A and II-B). This determines the required number of substrates and metal layers.

Table II presents the numbered zones, distances from the center of aperture to the middle of each zone, the required phase shift at the center of each zone, the selected UC# for each zone, the incident angle, and phase/insertion loss at the center of each zone. From Table II, it is assumed that the variations in phase shift and insertion loss for different incident angles are not significant for a lens with $f/D = 0.7$. It should be noted that variations in the insertion losses over the lens aperture might cause the same effect as nonuniform magnitude of feeds in a phased antenna array, leading to beam deformation related to beam width, side lobes, and so on. In order to cover 2-D spherical EM waves, the distribution of the unit cells emulates a ring-shaped topology, as illustrated in Fig. 9. It should be noted that the different gray zones in the patches represent different zones. In order to analyze the performance of the proposed lens thoroughly, full-wave EM simulations are performed for the entire lens structure.

Figs. 10 and 11 present the analyzed electric field distributions and the focal gains with the incident plane waves steered in different angles from the left side. It is observed that when the steered angles of the incident plane waves are 15° and 30°, the steered angles of the outbound spherical waves are larger than those of the incident plane waves and calculated to be 18° and 34.2°, respectively. Applying (18)

TABLE II

NUMBERED ZONES, DISTANCES FROM THE CENTER OF THE APERTURE TO THE MIDDLE OF EACH ZONE, THE REQUIRED PHASE SHIFT AT THE CENTER OF EACH ZONE, THE SELECTED UC# FOR EACH ZONE, INCIDENT ANGLE, AND PHASE AND INSERTION LOSS AT THE CENTER OF EACH ZONE

Zone#	Number of cascaded unit celles	Distance from the center of aperture to the middle of each zone (mm)	Required phase shift in the middle of each zone (deg)	Selected UC#	Incident angle in the middle of each zone (deg)	Phase of unit cell with normal incidence (deg)	Phase of unit cell in the middle of each zone (deg)	Insertion loss of unit cell with normal incidence (dB)	Insertion loss of unit cell in the middle of each zone (dB)
1	3	0	-274	1	0	-278	-278	1.8	1.8
2	3	7.2	-259	2	11.6	-262	-260	1.6	1.6
3	2	11.2	-236	3	17.7	-247	-244	1	1.1
4	2	14.4	-212	4	22.4	-211	-209	0.4	0.4
5	2	17.6	-182	5	26.7	-192	-188	0.8	0.9
6	2	20.8	-139	7	30.7	-145	-139	0.5	0.6
7	2	24	-101	9	34.4	-114	-107	1.5	1.7

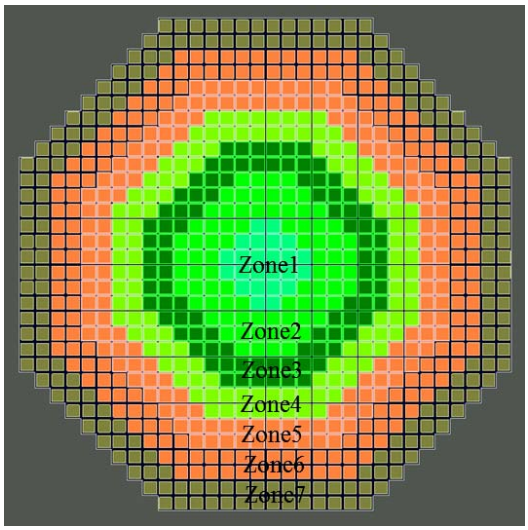

Fig. 9. Top view of the proposed lens employing mixed-order elliptic spatial filter arrays.

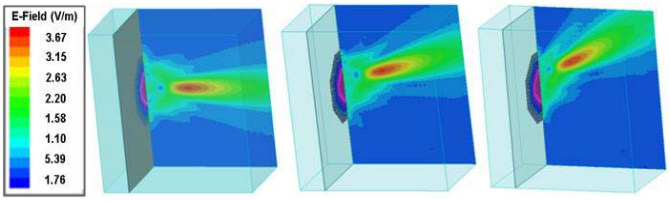

Fig. 10. 2-D electric field distributions of the incident plane waves steered in different angles from the left side. (a) 0°, (a) 15°, and 30°.

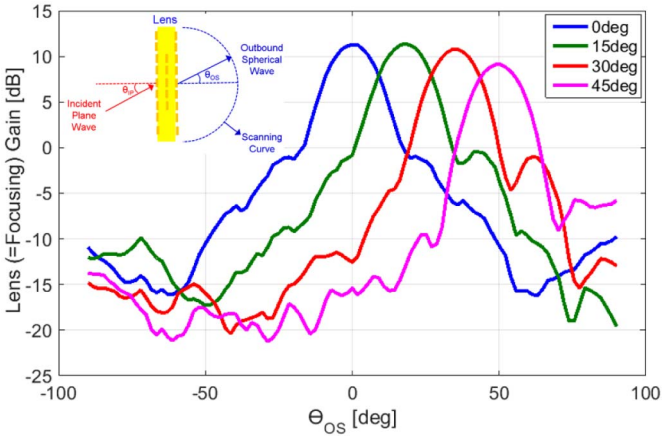

Fig. 11. Focal gains with the incident plane waves steered in different angles.

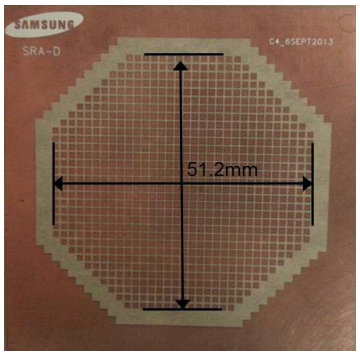

Fig. 12. Top view of the fabricated lens employing mixed-order elliptic spatial filter arrays.

in [14] for the simulation setup shown in Fig. 11, $\sin\Theta_{OS}/\sin\Theta_{IP} = 1/(1-K)$, where $K > 0$ is derived. For $0° < \Theta_{OS}, \Theta_{IP} < 90°$, this suggests that Θ_{OS} is always larger than Θ_{IP}. In the EM radiation mechanism of the lens antenna where wave propagation is in the opposite direction to that of the simulation model, in Fig. 10, the above incident plane wave becomes the outbound wave and the above outbound spherical wave becomes the incident wave.

III. Measurement

A. Fabrication and Measurement Setup

The proposed lens employing mixed-order elliptic spatial filter arrays is fabricated and tested in a relevant measurement setup. According to the simulated design in the previous sections, two substrates are selected as Rogers 6010 with a thickness of 0.25 mm and a bonding layer is selected as Rogers 2929 with a thickness of 0.05 mm. The top view of the fabricated sample is shown in Fig. 12. Fig. 13 shows the measurement setup where the proposed lens fed by a $\lambda/2$ dipole antenna is used as the Tx and a standard gain horn antenna is used as the Rx. The fabricated lens is mounted on a styrofoam plate, and the styrofoam plate is mounted on a polycarbonate holder. A $\lambda/2$ dipole antenna is positioned behind the lens as a source, in appropriate alignment with the lens. The polycarbonate holder is designed to enable changes in the distance between the antenna and the lens and changes in the steered angle of the incident plane wave.

B. Measurement Results

In order to accurately assess the focal distance of the proposed antenna, the distance between the antenna and the lens is varied and

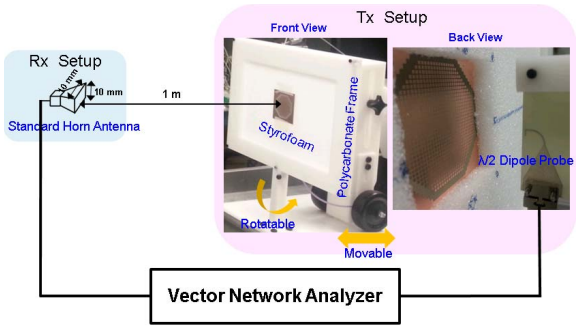

Fig. 13. Measurement setup: Tx setup (lens, polycarbonate frame, and a $\lambda/2$ dipole probe antenna) and Rx Setup (standard horn antenna) connected through vector network analyzer.

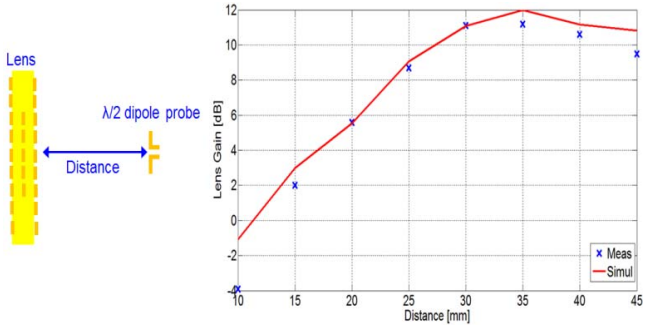

Fig. 14. Measured and simulated lens gain as a function of the distance between the lens and the $\lambda/2$ dipole probe antenna (antenna source).

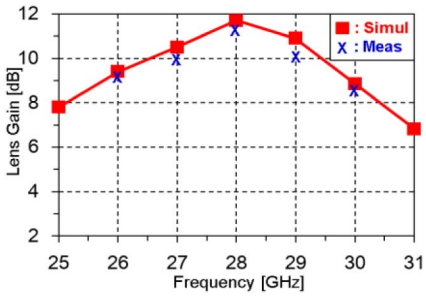

Fig. 15. Simulated and measured lens gain as a function of the frequency.

the gain of the lens is determined for each distance. The gain of the lens is obtained by measuring the received power before and after mounting the lens in front of the $\lambda/2$ dipole probe antenna. Fig. 14 presents the measured and simulated gain of the lens as a function of the distance between the antenna and the lens. The result of the measurement is in agreement with the corresponding simulated result. The peak gain of the lens is observed to be 11 and 12 dB from the measurement and simulation results, respectively. Fig. 15 shows the simulated and measured gain of the lens as a function of frequency. Less than 3-dB gain variation is observed over the frequency range 26–30 GHz, for the proposed lens having an electrically thin configuration ($\approx$0.05 λ_0). This suggests that structural discontinuity resulted from partial removal of the second metal layer does not cause phase distortions in the transition between different-order elliptic spatial filters, providing stable dispersion characteristics. In this frequency response, the gain of the lens is observed to vary from 9 to 12 dB. While in the simulation setup of Fig. 11, the incident plane waves are steered to be 0°, 15°, and 30°, in the measurement setup of Fig. 16, the incident spherical waves emitted from the $\lambda/2$ dipole antenna are steered. Therefore, as discussed in Section II-C, the measured steered angle of the outbound plane

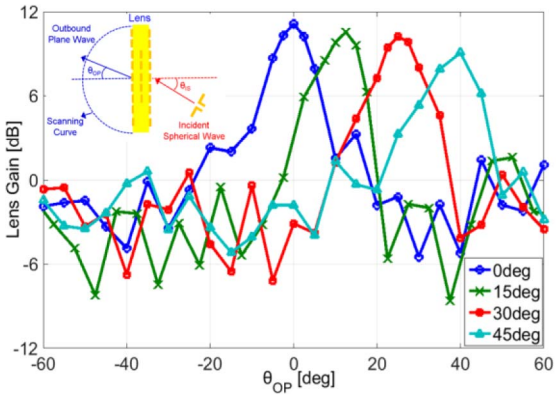

Fig. 16. Radiation patterns for the oblique incident spherical waves at different angles (0°, 15°, 30°, and 45°).

TABLE III
FEATURE COMPARISON BETWEEN PRIOR LENSES AND THE PROPOSED LENS

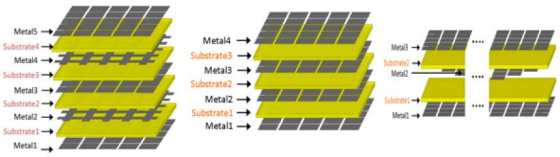

	Bandpass Lens in [8]	Lowpass Lens in [13]	Mixed-order Elliptic Lens
Number of Metal Layers	5	4	3
Number of Substrate Layers	4	3	2
Tunable Range of Phase Shift	170 deg	170 deg	170 deg
Size of D	186mm X 234mm (=6.2λ_0 X 7.8λ_0 at 10GHz)	186mm X 186mm (=5.3λ_0 X 5.3λ_0 at 8.5GHz)	51.2mm X 51.2mm (=4.8λ_0 X 4.8λ_0 at 28GHz)
Thickness	2.3mm (=0.08λ_0 at 10GHz)	9.8mm (=0.28λ_0 at 8.5GHz)	0.55mm (=0.05λ_0 at 28GHz)
f/D	1.2	1.0	0.7
Len Gain	9.6dB	10 dB	11.2dB
Bandwidth	19.20%	50%	15%

*f is the focal length and D is the aperture size of the lens

waves (steered angle of the plane waves) is smaller than that of the incident spherical waves emitted from the $\lambda/2$ dipole probe antenna. Fig. 16 illustrates the far-field radiation patterns for oblique incident spherical waves for each of the corresponding angles (0°, 15°, 30°, and 45°). The radiation patterns are obtained by subtracting the radiation patterns without the lens from the corresponding radiation patterns with the lens. As discussed earlier, the steered angles of the outbound plane waves are observed to be smaller than the steered angle of the incident spherical waves.

IV. BENCH MARKING

This section presents a comparison between the proposed lens and prior works of the thin lens utilizing uniform-order FSS responses [8], [13]. Table III compares the physical dimensions and the related performance characteristics of the aforementioned lenses. This comparison confirms the advantage of the proposed design approach. The advantage of the presented mixed-order elliptic filter array is that the proposed lens requires fewer substrates and metal layers than the prior works, to achieve the same tunable range of the phase shift (≈170°). In addition, it is found that employing the proposed mixed-order approach can render even smaller values of f/D (= 0.7) in comparison with the previous studies, exhibiting a higher lens gain for the given aperture. This indicates that the proposed design approach can be utilized to achieve a reliable focusing capability and fabrication tolerance/cost owing to a reduction in the number of required substrates and bonding and metal layers. This advantage of the proposed design approach can be very critical for situations and applications employing extremely high operating frequencies. It should be noted that the differences in the bandwidths of the lenses in Table III result from differences in the volume of the lenses.

V. CONCLUSION

A novel design approach enabling a reduction in the required number of substrates and bonding and metal layers for similar levels of lens focusing, compared with prior works, is introduced in this communication. The approach employs interlayer coupling between the top and bottom patches, rendering an elliptic filter response and mixed-order configurations of the elliptic filter unit cells. It is shown that the approach can produce an affordable 28-GHz thin lens. The proposed design approach is more promising for higher frequency applications where fabrication conditions become more challenging with complex multilayer configurations.

ACKNOWLEDGMENT

The author would like to thank Dr. W. Hong for his advisory support.

REFERENCES

[1] J. R. Costa, E. B. Lima, and C. A. Fernandes, "Compact beam-steerable lens antenna for 60-GHz wireless communications," *IEEE Trans. Antennas Propag.*, vol. 57, no. 10, pp. 2926–2933, Oct. 2009.

[2] J. Thornton, "Properties of spherical lens antennas for high altitude platform communications," in *Proc. 6th Eur. Workshop Mobile/Pers. Satcoms, 2nd Adv. Satellite Mobile Syst. (EMPS&ASMS)*, Sep. 2004, pp. 1–8.

[3] B. Chantraine-Bares, R. Sauleau, L. Le Coq, and K. Mahdjoubi, "A new accurate design method for millimeter-wave homogeneous dielectric substrate lens antennas of arbitrary shape," *IEEE Trans. Antennas Propag.*, vol. 53, no. 3, pp. 1069–1082, Mar. 2005.

[4] M. G. M. V. Silveirinha and C. A. Fernandes, "Shaped double-shell dielectric lenses for wireless millimeter wave communications," in *IEEE AP-S Int. Symp. Dig.*, vol. 3. Jul. 2000, pp. 1674–1677.

[5] A. Abbaspour-Tamijani, K. Sarabandi, and G. M. Rebeiz, "Antenna–filter–antenna arrays as a class of bandpass frequency-selective surfaces," *IEEE Trans. Microw. Theory Techn.*, vol. 52, no. 8, pp. 1781–1789, Aug. 2004.

[6] A. Abbaspour-Tamijani, K. Sarabandi, and G. M. Rebeiz, "A millimetre-wave bandpass filter–lens array," *IET Microw. Antennas Propag.*, vol. 1, no. 2, pp. 388–395, Apr. 2007.

[7] N. Behdad and M. A. Al-Joumayly, "A generalized synthesis procedure for low-profile, frequency selective surfaces with odd-order bandpass responses," *IEEE Trans. Antennas Propag.*, vol. 58, no. 7, pp. 2460–2464, Jul. 2010.

[8] M. A. Al-Joumayly and N. Behdad, "Wideband planar microwave lenses using sub-wavelength spatial phase shifters," *IEEE Trans. Antennas Propag.*, vol. 59, no. 12, pp. 4542–4552, Dec. 2011.

[9] C. Pfeiffer and A. Grbic, "Millimeter-wave transmitarrays for wavefront and polarization control," *IEEE Trans. Microw. Theory Techn.*, vol. 61, no. 12, pp. 4407–4417, Dec. 2013.

[10] N. Gagnon, A. Petosa, and D. A. McNamara, "Printed hybrid lens antenna," *IEEE Trans. Antennas Propag.*, vol. 60, no. 5, pp. 2514–2518, May 2012.

[11] A. I. Zverev, *Handbook of Filter Synthesis*. New York, NY, USA: Wiley, 1967.

[12] M. A. Al-Joumayly and N. Behdad, "A generalized method for synthesizing low-profile, band-pass frequency selective surfaces with non-resonant constituting elements," *IEEE Trans. Antennas Propag.*, vol. 58, no. 12, pp. 4033–4041, Dec. 2010.

[13] M. Li and N. Behdad, "Wideband true-time-delay microwave lenses based on metallo-dielectric and all-dielectric lowpass frequency selective surfaces," *IEEE Trans. Antennas Propag.*, vol. 61, no. 8, pp. 4109–4119, Aug. 2013.

[14] A. Abbaspour-Tamijani, L. Zhang, and H. K. Pan, "Enhancing the directivity of phased array antennas using lens-arrays," *Prog. Electromagn. Res. M*, vol. 29, pp. 41–64, Feb. 2013.